North–South Precipitation Patterns in Western North America on Interannual-to-Decadal Timescales

MICHAEL D. DETTINGER

U.S. Geological Survey, Scripps Institution of Oceanography, La Jolla, California

DANIEL R. CAYAN

U.S. Geological Survey and Climate Research Division, Scripps Institution of Oceanography, La Jolla, California

HENRY F. DIAZ

NOAA/ERL/CDC, Boulder, Colorado

DAVID M. MEKO

Laboratory for Tree-Ring Research, The University of Arizona, Tucson, Arizona

(Manuscript received 6 February 1997, in final form 20 May 1998)

ABSTRACT

The overall amount of precipitation deposited along the West Coast and western cordillera of North America from 25° to 55°N varies from year to year, and superimposed on this domain-average variability are varying north–south contrasts on timescales from at least interannual to interdecadal. In order to better understand the north–south precipitation contrasts, their interannual and decadal variations are studied in terms of how much they affect overall precipitation amounts and how they are related to large-scale climatic patterns. Spatial empirical orthogonal functions (EOFs) and spatial moments (domain average, central latitude, and latitudinal spread) of zonally averaged precipitation anomalies along the westernmost parts of North America are analyzed, and each is correlated with global sea level pressure (SLP) and sea surface temperature series, on interannual (defined here as 3–7 yr) and decadal (>7 yr) timescales. The interannual band considered here corresponds to timescales that are particularly strong in tropical climate variations and thus is expected to contain much precipitation variability that is related to El Niño–Southern Oscillation; the decadal scale is defined so as to capture the whole range of long-term climatic variations affecting western North America.

Zonal EOFs of the interannual and decadal filtered versions of the zonal-precipitation series are remarkably similar. At both timescales, two leading EOFs describe 1) a north–south seesaw of precipitation pivoting near 40°N and 2) variations in precipitation near 40°N, respectively. The amount of overall precipitation variability is only about 10% of the mean and is largely determined by precipitation variations around 40°–45°N and most consistently influenced by nearby circulation patterns; in this sense, domain-average precipitation is closely related to the second EOF. The central latitude and latitudinal spread of precipitation distributions are strongly influenced by precipitation variations in the southern parts of western North America and are closely related to the first EOF. Central latitude of precipitation moves south (north) with tropical warming (cooling) in association with midlatitude western Pacific SLP variations, on both interannual and decadal timescales. Regional patterns and zonal averages of precipitation-sensitive tree-ring series are used to corroborate these patterns and to extend them into the past and appear to share much long- and short-term information with the instrumentally based zonal precipitation EOFs and moments.

1. Introduction

Although precipitation is dominantly episodic, there are low-frequency controls that modulate it on multiyear timescales with frequently severe consequences for our society. In the last two decades, for example, North America has experienced several prolonged episodes of extreme drought and severe wet spells that have resulted in losses for the economies of the western United States. In California alone, the droughts of 1976–77 and 1987–92 are estimated to have resulted in over $2.6 billion in (unadjusted) losses (California Department of Water Resources 1978) and well over $3 billion (Gleick and

Corresponding author address: Dr. Michael D. Dettinger, U.S. Geological Survey, Scripps Institution of Oceanography, 9500 Gilman Drive, Dept. 0224, La Jolla, CA 92093-0224.
E-mail: mddettin@usgs.gov

Nash 1991) in costs, respectively. Flooding from persistently wet winter conditions is typically more episodic but can cause equally large damages; for example, floods along the West Coast resulted in damages of from $1 billion to $3 billion each winter from 1994–95 to 1996–97 (e.g., Lott et al. 1997). The combination of major floods in 1986 followed by the prolonged 1987–92 drought in California also led to the low-diversity/high-salinity conditions in San Francisco Bay that facilitated disruptions of bay ecosystems by the Asian clam *Potmocorbula amurensis* (Nichols et al. 1990), and the same prolonged drought caused widespread deaths of trees (30%–80%) in the Sierra Nevada (Gleick and Nash 1991). It is clear, in this context, that interannual and decadal precipitation variability plays major societal and ecological roles in western North America.

One of the notable characteristics of precipitation variability in western North America is the contrasting variation (or seesaw) of precipitation between the northwest and the southwest. When one region is wet, the other tends to be dry (e.g., Kiladis and Diaz 1989; Cayan and Webb 1992). This seesaw opposition of wet and dry conditions appears in analyses on many timescales and raises the following questions: 1) Is precipitation variability at decadal timescales simply a telescoped version of the variability on the interannual and even shorter timescales, or do the different precipitation timescales correspond to different processes and teleconnections? 2) Do the north–south precipitation patterns reflect changes in the overall amount of precipitation delivered to the cordillera of North America, or, if instead they are redistributions of the same precipitation, what form do those redistributions characteristically take? Answers to these questions bear directly on how, and to what extent, long-term precipitation variations in the American west can be predicted and managed. If decadal precipitation variation is a simple sum of interannual and faster climate processes, then we can predict decadal precipitation only as well as our longest term interannual projections. If, however, decadal precipitation variations arise from a separate decadal climate dynamics, then long-term predictions hinge on understanding of the climate processes at each of several timescales, with improvements possible in each.

In this paper, we examine precipitation and related climate variability in western North America over the last 110 yr. The north–south seesaw of seasonal precipitation that has been observed at interannual and longer timescales is characterized by studying the behavior of zonal averages of precipitation over western North America on interannual and decadal timescales. The study of zonally averaged precipitation anomalies was motivated by the characteristically zonal patterns of precipitation (e.g., Cayan and Webb 1992) that correspond to El Niño–La Niña (warm and cool phases of the ENSO phenomenon of the tropical Pacific; Philander 1990) influences in the western United States, by the broad east–west extents of precipitation patterns in western North America associated with decadal variations of the North Pacific (Latif and Barnett 1996; Ting et al. 1996), and by various results on seasonal timescales that show similarly zonal precipitation patterns (e.g., Brown 1995; Mitchell and Blier 1997). A principal component analysis (PCA) of areal patterns of decadal precipitation variation in western North America is presented in a companion paper (Cayan et al. 1998) and validates the importance of three centers of action in precipitation west of the Rocky Mountain cordillera identified here (near 50°N, near 40°N, and near 30°N).

Spatial moments (overall average, center of mass, and spread) of the year-to-year zonal precipitation patterns are investigated to characterize variations of the precipitation delivered to western North America and north–south placement of precipitation anomalies on interannual and longer timescales. Sea level pressure (SLP) and sea surface temperature (SST) patterns over the analysis period are examined as a means to identify the climatic forcings associated with precipitation changes at the different timescales. Finally, a partial verification of the long-term representativeness of precipitation patterns and an extension of the preinstrumental zonal average precipitation record are developed using tree-ring chronologies that cover the same space and timescales as the precipitation series.

2. Data

Four primary datasets are used. Zonal averages of the gridded historical precipitation anomalies of Eischeid et al. (1991) and Eischeid et al. (1995) were used to investigate the north–south variations that characterize western North American precipitation, such as those that might be associated with shifts in regional storm tracks. The global set of gridded precipitation anomalies were interpolated onto a 5° lat × 5° long grid from monthly precipitation deviations from period-of-record mean monthly precipitation totals at 5328 stations. The station records were individually tested and visually inspected for discontinuities and other nonclimatic biases as described by Eischeid et al. (1991). Preparation and quality control of the station and gridded data are described in the original reference. Updates to this dataset are described by Eischeid et al. (1995). In the mountainous terrain of western North America, a majority of weather stations are located at lower altitudes so that the present analyses probably also have a low-altitude bias. The use of precipitation anomalies in the present analyses may help to reduce the influence of this bias. Indeed, the regional patterns found here are partially corroborated by tree-ring series (which tend to be from higher altitudes) and, in a companion paper, Cayan et al. (1998) find that regional precipitation patterns in the Eischeid et al. (1991) data are in good agreement with snowpack and streamflow data.

In this study, anomalies from grid cells extending from the west coast of North America to 650 km inland

were averaged along each of seven (zonal) rows of the grid, from 25° to 55°N, and the resulting zonal averages were temporally averaged for each November–April cool season from 1880–1994. Results did not change appreciably when 10 rows from 15° to 60°N were analyzed instead; however, because the southernmost and northernmost precipitation gridpoint time series began later than the rest, analyses from the array from 25° to 55°N are discussed here in most cases.

Precipitation variability in western North America has links to atmospheric circulations over the North Pacific and North America as well as to circulations on global scales (Cayan et al. 1998). Therefore, gridded SLP anomalies are correlated to spatial statistics of zonal precipitation variation to delineate atmospheric-circulation patterns to which precipitation responds. SLP anomalies were obtained from the Scripps Institution of Oceanography in the form of monthly deviations from 1951–92 monthly means on a 5° lat × 5° long grid from 42.5°S to 72.5°N. This near-global anomaly set was developed with data from the U.S. National Meteorological Center, the U.S. Navy Fleet Numerical Oceanography Center (Monterey, California), and the Australian, New Zealand, and South African meteorological bureaus (as described by Barnett et al. 1984, and updated since). To verify correlation patterns found in these near-global SLPs for periods before their 1951 beginning, gridded monthly SLPs from 1899 on, on a 5° diamond grid over the Northern Hemisphere (NH), were analyzed also. The monthly NH SLPs are from the National Center for Atmospheric Research (Trenberth and Paolino 1980) and from the National Oceanic and Atmospheric Administration's (NOAA) Climate Analysis Center.

Connections also appear to exist between precipitation variations and sea surface temperature (SST) variations in the Pacific Ocean and beyond (Cayan et al. 1998). Similar connections between SSTs and continental precipitation have been identified on synoptic to decadal scales in the Atlantic basin (Zorita et al. 1992; Hurrell 1995). Therefore, SST anomalies are analyzed here to delineate regional and global climate linkages to precipitation. SST anomalies from the 5° × 5° global gridded GISST adjusted-anomaly SST set from the Hadley Centre (Parker et al. 1995) are correlated with the zonal-precipitation statistics from 1901–91.

Finally, historical precipitation and SST series for the North Pacific–North American region are only about 100 yr long, which is a relatively short period with which to quantify the decadal modes and infrequent forms of precipitation variation identified here. Therefore, to establish whether decadal modes from the instrumental record are robust with time, a set of tree-ring chronologies within 5° latitude belts corresponding to the precipitation zones described above were selected from the national tree-ring network of Meko et al. (1993) and from Mexican and Canadian sites. The tree-ring chronologies were chosen from sites that were expected to be precipitation sensitive in the westernmost Rocky Mountains belts. Tree-growth chronologies from 1708 to 1965 were standardized and averaged in each latitude zone to obtain ''zonal tree-ring'' series corresponding to the zonal-precipitation series. The tree-ring analogs of the north–south precipitation patterns are characterized in another subset of Meko et al. (1993) tree-ring network by temporal and spatial correlation to variations of the north–south precipitation patterns. This subset was culled from the original 250-site network used by Meko et al. (1993) to reduce the densely clustered sites in the southwestern states, preventing that region from overwhelming the spatial analyses. Where site locations were unusually dense, nearby chronologies were averaged. A few sites in data-rich areas were dropped. In the Southwest where different species have strongly related ring patterns, averaging was done without concern for species. In the northwest, averaging was restricted to chronologies of the same species.

3. Methods

Cool-season precipitation (November–April) is the focus of the present study because most of the annual precipitation over a large part of the study area occurs during these months. Although spectral analyses of precipitation in western North America indicated concentrations of power and periodicity at numerous frequencies, these variations are not sufficiently distinct nor reliable to support distinct interpretations. Therefore, in the present analyses, two relatively broad bands are considered, with the objective of better understanding whether precipitation variations on interannual and decadal scales have different spatial patterns or climatic-forcing regions. The two broad timescales of precipitation variability addressed are an interannual timescale chosen here to cover a spectral window between 3 yr^{-1} and 7 yr^{-1}, and a ''decadal'' window that emphasizes precipitation variability that is slower than 7 yr^{-1}. Precipitation anomalies were time-filtered prior to some of the analyses with bandpass and low-pass filters (Kaylor 1977) with half-power points at 3 and 7 yr^{-1}, and at 7 yr^{-1}, respectively, to isolate variations in these arbitrary bands. The filters used have sharp responses so that they pass 99% of power for frequencies faster than 6.1 yr^{-1} and slower than 4.1 yr^{-1} for interannual variations, and slower than 8.0 yr^{-1} for decadal variations; less than 1% of power is passed for frequencies slower than 7.7 yr^{-1} and faster than 2.9 yr^{-1} for interannual and faster than 6.2 yr^{-1} for decadal variations.

The interannual 3–7-yr timescale is analyzed here because the El Niño–Southern Oscillation (ENSO) (Diaz and Markgraf 1992) contains variations that are concentrated in and around this range. Although ENSO has variations both faster and slower than this band, the 3–7-yr range is particularly strong in the Tropics (e.g., Jiang et al. 1995; White and Tourre 1995). One consequence of filtering to remove the higher-frequency (<3 yr^{-1}) variations is that the effects of individual El

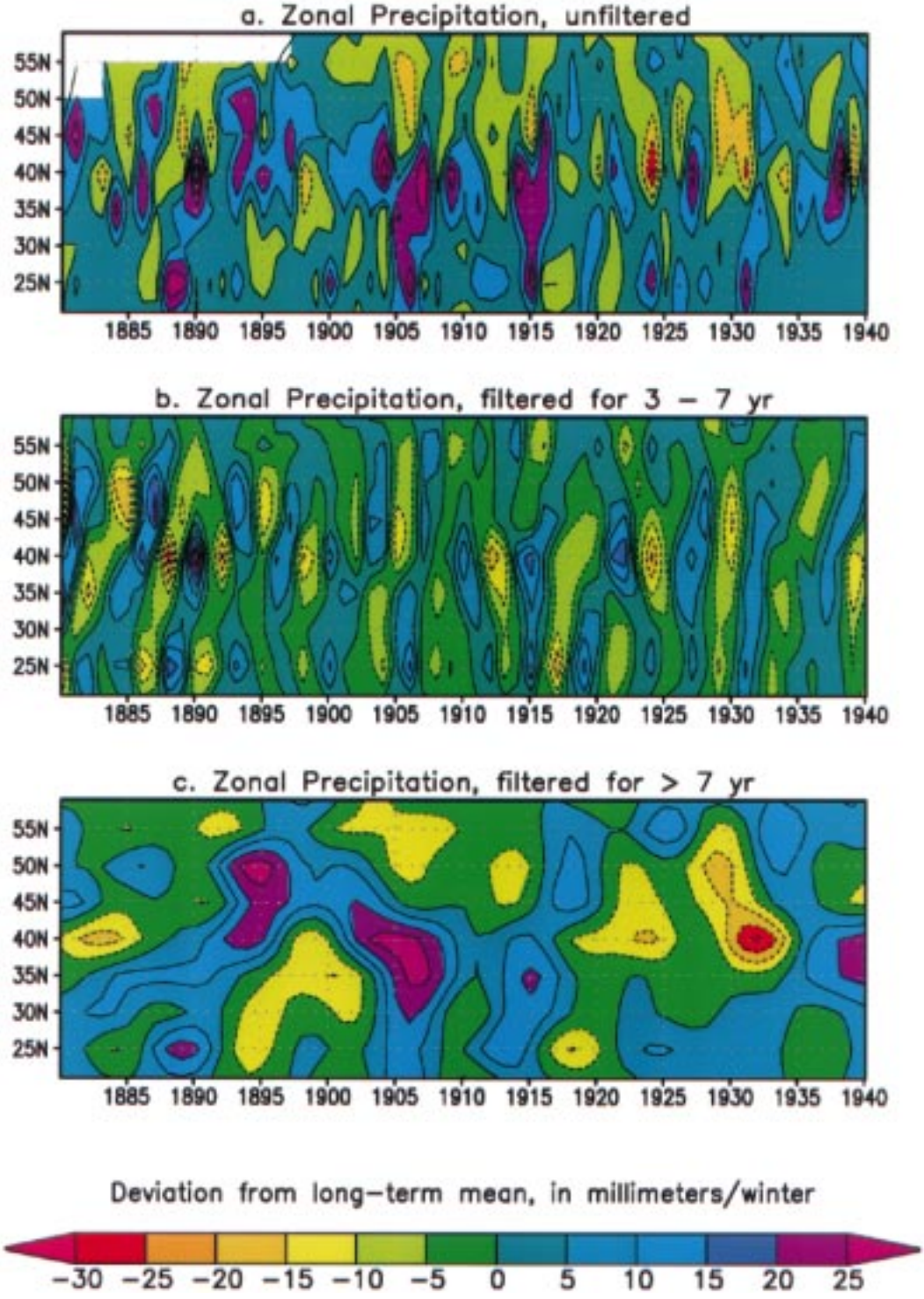

FIG. 1. Time–latitude diagrams of zonal November–April precipitation averages, 1880–1994: (a) unfiltered, (b) filtered for 3–7 yr (interannual) variability, and (c) filtered for >7 yr (decadal) variability.

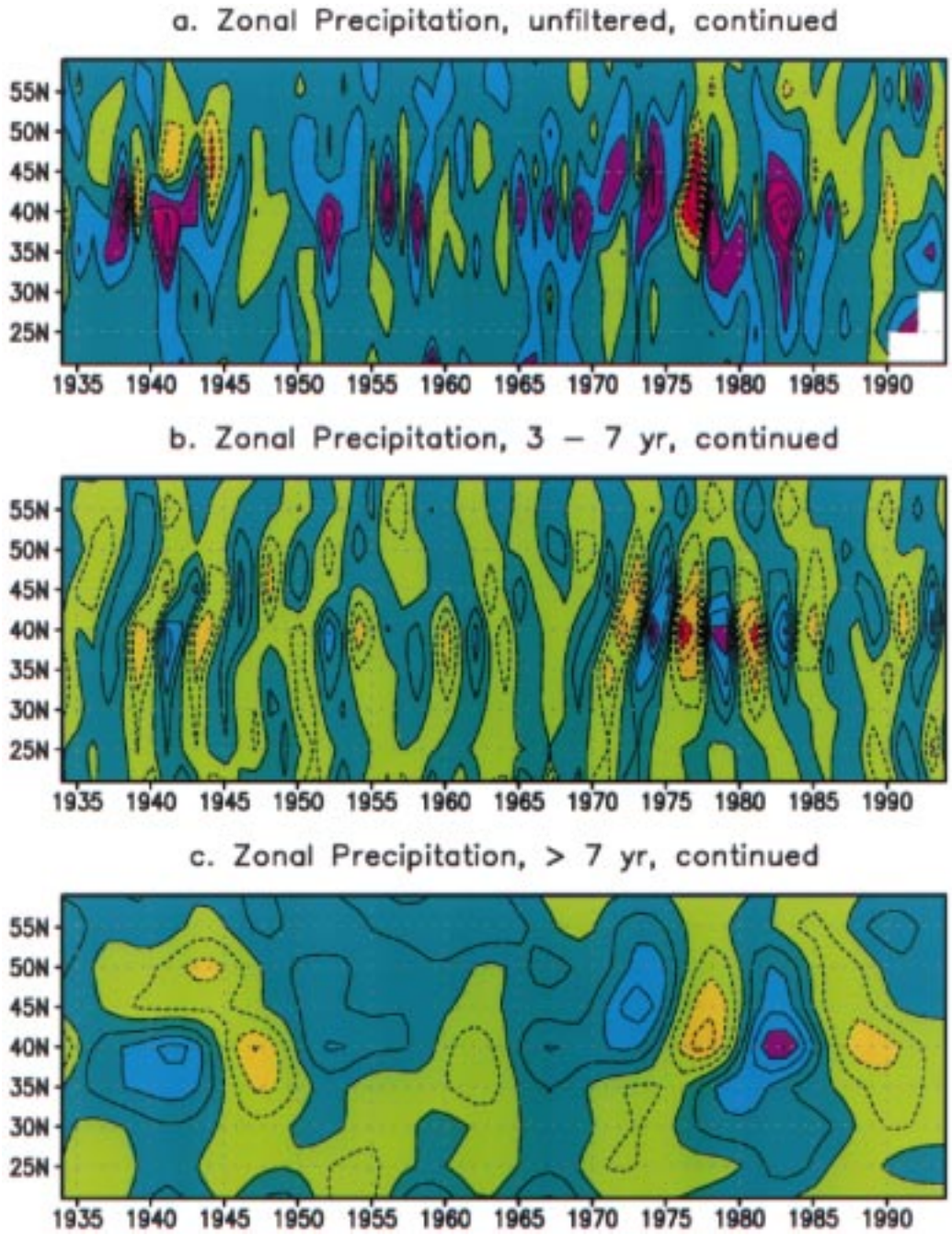

FIG. 1. (*Continued*)

Niño and La Niña events are almost lost (as will be indicated later).

A spatial PCA of zonal profiles of the filtered precipitation anomalies was used to develop unrotated empirical orthogonal functions (EOFs) that describe dominant spatial variations at each timescale. Spectral peaks in univariate series are characterized in this paper by the maximum entropy method (MEM) and tested for significance by the multitaper method (MTM) (Dettinger et al. 1995b). The nonadaptive F-distribution statistical test used with MTM identifies significantly periodic variations, which are not necessarily the most powerful variations (Percival and Walden 1993, 512; Lees and Park 1995).

Various indices of the north–south patterns of precipitation, on both interannual and decadal scales, were correlated with gridded SLP and SST series. Maps of the correlations are used to diagnose climate-system

TABLE 1. Variance of zonally averaged precipitation in unfiltered, interannual, and decadal bands.

Center of zone	Unfiltered (mm month^{-1})^2	Interannual variance (%)	Decadal variance (%)
55°N	74	32	32
50°N	104	39	38
45°N	190	37	22
40°N	395	33	27
35°N	150	37	29
30°N	52	35	33
25°N	112	41	18
25°–55°N	1077	26	20

connections that drive the precipitation patterns. Particularly in the case of decadal variations, too few realizations of the patterns are available from the instrumental records to afford much certainty. Therefore, correlation maps are plotted without much regard for their local levels of statistical confidence and should be viewed only as suggestions of the links that may exist. However, in order to assess the overall levels of significance of the correlation patterns, correlation maps also were constructed from 1000 sets of SLP and SST maps chosen at random, in 1-yr sequences, from the historical record and then filtered as in the ''real'' correlation analyses. The number of correlation maps based on this filtered random sequences that had more (or less) grid points with correlations above various thresholds than the observed correlation maps are assessed to determine which maps and which regions are significantly correlated with the interannual and decadal precipitation signals.

4. Zonal precipitation patterns

a. Variance

Zonally averaged, cool-season precipitation anomalies over western North America are plotted as a function of latitude and time for 1880–1994 in Fig. 1a. Bandpass and low-pass filtered versions of the same anomalies are shown in panels b and c. Overall, 26% of zonal-precipitation variance is present in the interannual anomalies (Fig. 1b) and 20% is in the decadal anomalies (Fig. 1c). The remaining 54% of variance has periods less than 3 yr. The relative contributions of interannual and decadal fluctuations to the total variance are listed, by latitude, in Table 1. Precipitation in the middle latitudes (35°–45°N) and, especially, the near-tropical (near 25°N) zones have relatively less decadal variance than interannual variance.

In the unfiltered series, as well as in both filtered series, precipitation anomalies at 45° and 50°N are highly correlated with each other ($r = +0.8$ in unfiltered series) and are moderately anticorrelated overall with anomalies at 30° and 35°N ($r = -0.4$). To better understand and compare these north–south dipoles, a spatial PCA was used to isolate the dominant modes of spatial variation in variously filtered versions of the zonal-average precipitation series. These dominant patterns (described briefly in the next subsection) suggested the use of spatial moments of zonal precipitation to address the issues of overall precipitation variability and the similarities of interannual and decadal precipitation patterns. In interests of brevity, the spatial moments will be the focus of this paper.

b. Spatial EOF analysis

EOFs were derived from spatial PCA of zonal-precipitation anomalies on several different timescales. EOFs of zonal interannual (3–7 yr) and decadal (>7 yr) precipitation anomalies are shown in Fig. 2. Also computed, but not shown here, were EOFs of high-frequency (1–3 yr) and lower-frequency (>10 yr) anomalies. Interestingly, the leading EOFs in all of these frequency bands are dominated by loading patterns (spatial distributions) that are quite similar to the interannual and decadal patterns. This similarity indicates that the north–south precipitation patterns isolated in the EOF analyses either 1) are frequency independent like white noise—that is, they do not fall distinctly into one or the other of the frequency bands or 2) they share similar climatic driving forces and ''footprints'' in the precipitation field of western North America, or some combination of both.

The first two EOFs of the interannual zonal precipitation anomalies capture 29% and 22%, respectively, of the variance of the filtered series from 25° to 55°N (weights from a similar analysis between 15° to 60°N are shown in Figs. 2a and 2b for completeness). Interannual EOF 1 mostly captures precipitation-anomaly differences between the regions north and south of 40°N. Interannual EOF 2 captures precipitation-anomaly differences between regions from 35° to 50°N and the regions farther south and north. Time variations of these interannual precipitation modes are captured by the corresponding principal component (PC) series (not shown). Both interannual PC series are, of course, characterized by variations in the 3–7-yr range, but, specifically, PC 1 contains marked spectral peaks with periods around 4.2 and 5.3 yr (as estimated by both MEM and MTM, with 99% significance of MTM peaks), which it shares with PC 2 (significant at 95% level). The PC 2 also has a minor peak with period of about 3.5 yr (significant at 99% level). These frequencies will characterize most of the interannual indices analyzed in this paper. Particularly strong north–south precipitation contrasts are indicated by the large amplitudes (positive and negative) of PC 1 during the intervals 1905–20, 1935–45, and 1970–83. Particularly large excursions dominated precipitation near 40°–45°N, captured by PC 2, during 1917–32 and 1975–83. The overall spatial variance of precipitation changes from year to year also on roughly decadal timescales, and, for the most part, these first two EOFs capture those decadal fluctuations in interannual variance.

The leading spatial EOFs of the decadal, zonal precipitation anomalies are shown in Figs. 2c and 2d. These two modes capture 33% and 20% of the variance of the decadal filtered anomalies, respectively. Decadal EOF 1 captures precipitation differences between regions north and south of about 40°N and is very similar to the pattern captured by interannual EOF 1. Decadal EOF 2 captures precipitation differences between a broad region from 30° to 50°N and the bordering regions to the north and south. This pattern is reminiscent of interannual EOF 2. The general similarity of the leading spatial modes of interannual and decadal variations is in keeping with the similar spatial modes on the same two timescales observed by Cayan et al. (1998) in their analysis of gridded precipitation variations in western North America. The dominant periods of variation in decadal PC 1 (not shown) are about 14 and about 8.5 yr (as indicated by both MEM and MTM). Decadal PC 2 is characterized by variations on 16- and 8-yr time frames. No relations between the interannual and decadal PCs are evident, although, time intervals of large overall precipitation contrasts in the decadal series coincide, since about 1900, with correspondingly more variable periods in the interannual band. Thus these periods (e.g., centered at about 1905, 1915, 1930, and 1980) are periods of increased long-term *and* shorter term precipitation variability.

The EOFs in Fig. 2 were derived from cross-correlation matrices (rather than cross-covariance matrices) so that the relative amplitudes of precipitation series from zone to zone (Table 1) are not factored into the loading patterns. When the EOF weights are rescaled by the standard deviation of the filtered precipitation series at each zone, the sums of the EOF 1 weights from the midlatitudes from 25° to 55°N are +1 and +3 mm month^{-1} for decadal and interannual bands, respectively. Thus the net effects of both decadal and interannual EOFs 1 are small in terms of overall precipitation reaching western North America. These first EOFs represent north–south redistributions of precipitation more than changes in overall precipitation amounts. In contrast, the sums for decadal and interannual EOFs 2 are −12 and −8 mm month^{-1} for decadal and interannual bands, respectively. Thus, the net effects of the EOFs 2 are larger (especially in the decadal timescale) and they capture year-to-year differences in overall precipitation, with the most important contributions centered near 40°–45°N.

5. Zonal precipitation moments

With these characteristic patterns in mind, and in order to directly address our question of how much overall variation of precipitation to western North America is associated with the north–south precipitation fluctuations, three spatial moments were calculated from the unfiltered zonal-precipitation series. The moments used here are the first three precipitation-weighted moments of the zonal distributions in the unfiltered series; they are the domain-average precipitation for each winter ($\bar{p}$), the central latitude of each winter's precipitation distribution (c), and the latitudinal spread of the winter's precipitation distribution (s), with

$$\bar{p} = \left(\sum_{i=25N}^{55N} a_i p_i\right) \Bigg/ \left(\sum_{i=25N}^{55N} a_i\right),$$

$$c = \left(\sum_{i=25N}^{55N} i a_i p_i\right) \Bigg/ \left(\sum_{i=25N}^{55N} a_i p_i\right), \quad \text{and}$$

$$s = \left[\left(\sum_{i=25N}^{55N} (i - c)^2 a_i p_i\right) \Bigg/ \left(\sum_{i=25N}^{55N} a_i p_i\right)\right]^{1/2},$$

where p_i is the zonal-average winter-total precipitation at zone i, and a_i is the area covered by each zonal average. Zonal-average winter-total precipitation series were calculated by adding zonal averages of the grid-cell precipitation climatologies from Eischeid et al. (1991) to the corresponding anomalies that form the core of their dataset. Several approaches to constructing the zonal precipitation anomalies were tried, and aside from trends associated with changing networks in some methods, all gave similar results. The time series of the three statistics are shown in Fig. 3.

a. Variability of precipitation moments

Domain-average precipitation ($\bar{p}$) (see Fig. 3a) immediately shows how much the total precipitation in western North America varies from winter to winter. Notice that the general range is ±7–10 mm month^{-1} with a few extreme years (e.g., 1977, 1983) deviating from normal by as much as 20 mm month^{-1} (about 30% of the domain average precipitation). Distributed over the entire area covered by the zonal-precipitation averages, and over the entire 6-month ''winter'' considered here, the general range of variability amounts to about ±200 km^3 season^{-1} out of the long-term average total precipitation (1400 km^3 season^{-1}), or a little more than ±10% of the overall average. Particularly long sustained dry spells occurred in the 1920s and early 1930s and in the late 1980s, each of which reduced total precipitation in the study area by about 10% for several years. Otherwise, most excursions from the normal overall precipitation have been brief. The dry spell in the late 1980s is notable because it was long enough *and* variable enough so that both decadal and interannual timescales contributed all along the north–south domain (Figs. 1b and 1c). Otherwise, the domain-average series is perhaps most notable for its lack of trend and other low-frequency variations—compared to much larger low-frequency temperature variations illustrated in U.S. mean temperatures (Dettinger et al. 1995a) and North Pacific SSTs (Trenberth and Hurrell 1994). The domain-average time series shows considerable year-to-year variation, with spectral peaks around 15, 5.3, and

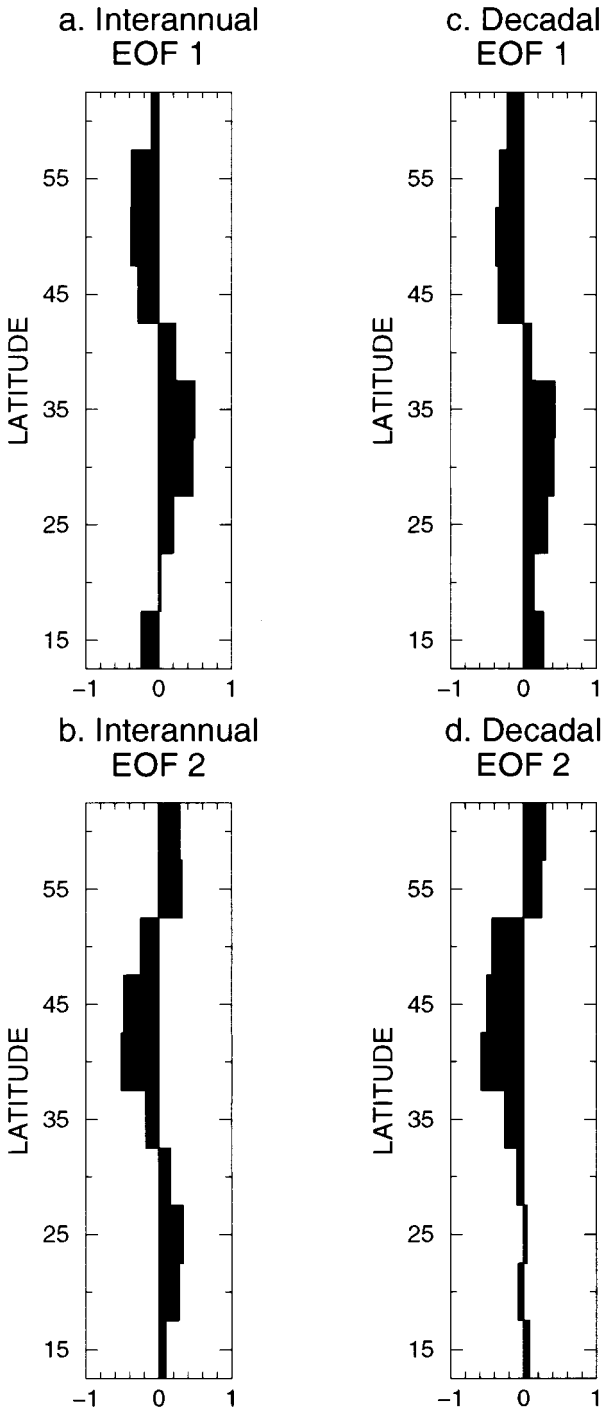

FIG. 2. Zonal-precipitation EOF loadings for interannual components (a) 1 and (b) 2, and for decadal components (c) 1 and (d) 2.

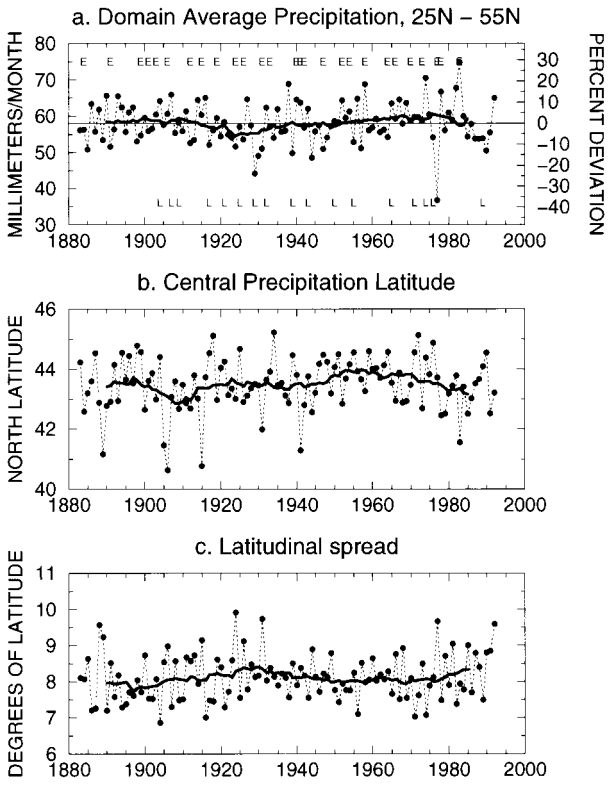

FIG. 3. (a) Domain-average precipitation, (b) central precipitation latitude, and (c) latitudinal spread, 1880–1994. See text for definitions. Here, ''E'' and ''L'' in (a) indicate El Niño and La Niña years (determined from extremes of the SOI), respectively. Heavy curves are 15-yr averages.

2.2 yr (at 95% significance levels by MTM) and around 4.3 and 3.4 yr (at somewhat less significant levels). These peaks were also found in the PC series associated with the interannual and decadal EOFs (Fig. 2).

Central precipitation latitude (*c*) (Fig. 3b) is a ''center of mass'' in the north–south direction of the spatial precipitation distributions for each winter. Coefficients of variation for the precipitation zones considered here range between 13% in the north and 30%–50% in the south, but overall are small enough so that *c* does not vary more than about $\pm 1°$–$2°$ in most years ($\sigma = 1°$ latitude). Much of this stability is due to the large climatological (mean) differences in precipitation from north to south that overwhelm year-to-year anomalous variations. Riehl (1981) also has argued, on the basis of thermal wind–kinetic energy conversions, that the position of the subtropical jet is fixed within 10° latitude across a wide range of temperature distributions and to a few degrees latitude under near-normal conditions. Thus north–south distributions of precipitation in western North America also may be limited by fairly narrow dynamical constraints.

The *c* series shares several of the spectral peaks found in the domain-average series, with peaks at 13, 5.3, 4.3, 3.2, and 2.4 yr. Several multiyear monotonic episodes of northward or southward movement of the central latitude are evident in Fig. 3b. In most cases, the progressive northward shifts seem to arise from multiyear shifts in the interannual band [e.g., the late 1960s–70s (Fig. 1b)], but the progressive shift during the late 1980s is more readily attributed to a drying (drought) that

TABLE 2. Correlations between unfiltered precipitation moments (1883–1992), decadal PCs 1 and 2 (1883–1992),* and the unfiltered SOI (1933–87). Bold where significantly different from zero at 99% level.

	$\bar{p}$	c	s	SOI
$\bar{p}$	1			
c	−0.18	1		
s	**−0.45**	**−0.45**	1	
SOI	−0.17	**+0.63**	−0.32	1
Decadal PC 1	+0.01	**−0.48**	+0.14	**−0.40**
Decadal PC 2	**−0.39**	+0.09	+0.31	+0.05

* Interannual PCs are not significantly correlated with the variables shown and decadal PCs are not correlated with each other.

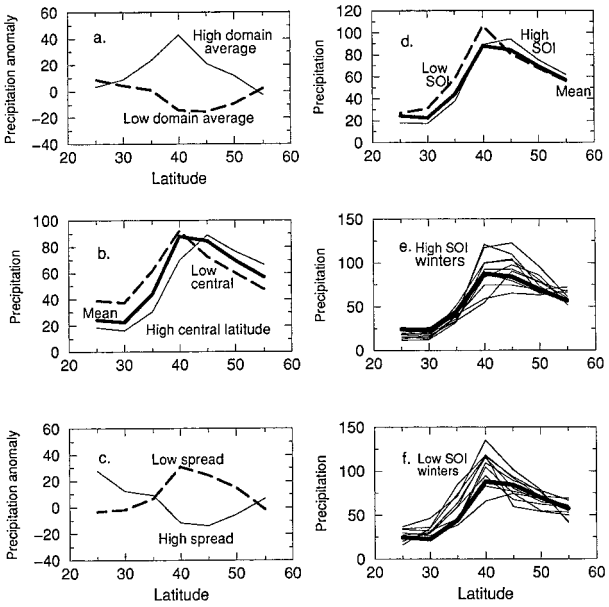

FIG. 4. (a)–(d) Average winter precipitation and precipitation anomalies by 5° latitude zone, western North America, during 1880–1994, in mm month^{-1}, for (a) the 10 yr with highest and lowest domain-average precipitation, (b) the 10 yr with highest and lowest central precipitation latitudes, (c) the 10 yr with highest and lowest latitudinal spreads, and (d) the 10 yr with highest and lowest SOI. (e)–(f) Winter precipitation totals, in mm month^{-1}, during each of the 10 yr with (e) highest SOI values and (f) lowest SOI values. Heavy curves in (b) and (d)–(f) are long-term average precipitation rates.

begins in the northwest and gradually intensifies and moves farther southward on the decadal scales (Figs. 1a,c, and Fig. 3b). This response is only broadly related to more frequent El Niños during the 1980s and instead may derive from a combination of El Niño influences and changes in the climate of the North Pacific basin (e.g., Ting et al. 1996; Latif and Barnett 1996). The El Niño years 1906, 1915, 1931, 1941, and 1983 (year +1's of events; Kiladis and Diaz 1989) have some of the lowest central-latitude values, whereas the highest central-latitude years (1918, 1925, 1934, 1972, and 1976) are neither El Niño nor La Niña years.

Finally, the latitudinal spread (s; Fig. 3c) is the weighted standard deviation of the zonal distribution of each winter's precipitation and represents an attempt to measure how focused and unimodal is the zonal precipitation pattern. As with the central latitude, latitudinal spread exhibits a rather small range. During most years, the spread is within 1° of its long-term average (~8°). Spectral peaks for latitudinal spread are found at 18, 6, 4.4, and 2.2–2.5 yr. The El Niño years of 1924, 1931, and 1977 are notable for their large latitudinal spreads, which derive from mostly unimodal anomaly patterns, that is, widespread dryness (Fig. 1a) due to persistent ridging along western North America.

Correlations between $\bar{p}$, c, s, and the Tahiti–Darwin SOI shown in Table 2 indicate that connections exist between $\bar{p}$ and s and between c and s. Of all the pairs of variables, the strongest connection is between c and SOI ($r = +0.63$), indicating that the central latitude of precipitation shifts southward when the Tropics are in their warm El Niño state and northward when the Tropics are in their cool La Niña state. Increases in precipitation in the southern part of the study area (which result in decreased central latitude) also result in increased latitudinal spread and in decreased overall precipitation. To clarify these relations, the average distributions of zonal precipitation during the winters with the 10 largest and 10 smallest values of $\bar{p}$, c, s, and SOI are shown in Fig. 4.

Notice first that domain-average precipitation is largest in years when precipitation near 40°N is large (Fig. 4a); domain average is smallest when precipitation is anomalously low from 40°–50°N. This relation is also indicated by the sums of EOF weights discussed earlier, by the correlation between $\bar{p}$ and decadal PC 2 (Table 2) and by correlations of $\bar{p}$ with the original gridded anomalies (not shown).

The central latitude c increases when conditions are wet in the north and dry in the south (Fig. 4b and later in Figs. 6a,d). Notice that the long-term average north–south distribution of zonal precipitation has a skewed appearance (heavy curve, Fig. 4b), with a maximum near 40°–45°N, a steep decline to the south and a slight decline to the north. With this distribution, if northern precipitation increases relative to southern precipitation, the central latitude increases while spread decreases (the distribution becomes more sharply peaked farther north, as in the solid curve of Fig. 4b). If southern precipitation increases relative to northern, then the distribution is flatter, spread increases, and the center moves south (as in the dashed curve). As expected from this argument, the years with largest latitudinal spread are characterized by reduced precipitation in the higher latitudes, especially around the precipitation maximum at 40°N, and increased precipitation in the south (as shown in Fig. 4c and inferred from Fig. 4b). As with the other two statistics, conditions at 40°N dominate this relation. When the interannual band is considered, the correlation between $\bar{p}$ and c approaches the 95% significance level ($r = -0.29$).

The strongest El Niños (large, negative SOI) exhibit precipitation increases in the south but, on average, not much effect on precipitation in the north (Fig. 4d). During the strongest La Niñas (SOI > 0), northern precipitation increases and, on average, southern precipitation decreases (Fig. 4d). These changes result in a strong linear correlation of central latitude c with SOI (Table 2). However, during high SOI, the southern precipitation deficits are smaller than the northern excesses so that, under both SOI extremes, when SOI < 0 *and* when SOI > 0, domain average precipitation increases. As a consequence, the linear correlation of $\overline{p}$ and SOI is weak (Table 2). This result is consistent with the observation that during both the largest El Niños and La Niñas, northern California and Oregon commonly are wetter than normal. The precipitation totals during each of the 10 highest and lowest SOI years, which were averaged to form Fig. 4d, are shown in Figs. 4e–f. South of about 40°N, La Niñas are consistently drier than normal (Fig. 4e) and El Niños are consistently wetter than normal (Fig. 4f). Farther north, La Niñas are most often wetter than normal but El Niños have had more varied outcomes. Thus, ENSO influence on precipitation in western North America includes some cases which could be called a north–south seesaw, but also includes cases with overall wetness. Conversely, not all cases of north–south precipitation contrasts are due to ENSO.

When the SOI correlations were recomputed using interannual and decadal components of $\overline{p}$, c, and s (not shown), the SOI–c correlation in Table 2 was found to derive nearly equally from the interannual and decadal bands. The almost-significant positive correlation between SOI and s derives exclusively from a strong decadal relation between the two ($r = +0.65$). Correlations of the precipitation moments and SOI with decadal PCs 1 and 2 also are presented in Table 2. As expected from the distribution of EOF weights (dry in north and wet in south when PC 1 is positive), decadal PC 1 is significantly anticorrelated with (unfiltered) c; the north–south seesaw of precipitation anomalies captured by EOF 1 captures mostly the same kind of north–south displacements measured by c. Decadal PC 1 also is anticorrelated with unfiltered SOI. Decadal PC 2 is anticorrelated with $\overline{p}$, as expected from the sums of EOF 2 weights (discussed earlier).

b. Climatic forcing of moments

To map the large-scale climatic conditions that are associated with the north–south precipitation variations described by the spatial moments, the moment series were filtered to isolate the interannual and decadal components, and then correlated with filtered, gridded SLPs from 1951–92 and gridded SSTs from 1880–1994. Correlations with gridded NH SLPs from 1899–1994 also were calculated (but are not shown here) to confirm the long-term stability of the NH part of the global SLP patterns discussed. Correlations between interannual $\overline{p}$ and SLP are weak overall (Fig. 5a), as indicated by the pattern significance test described in section 3. The correlations are notably weak in the Tropics (in keeping with the lack of $\overline{p}$ correlation with SOI) and suggest that $\overline{p}$ responds, on interannual timescales, to the local influence of circulation anomalies directly over and offshore from the 40°–45°N part of western North America. As with the circulation patterns associated with the closely related California precipitation mode (Cayan et al. 1998), regional circulation influences on $\overline{p}$ are too varied to be captured in a single set of correlation coefficients. Correlations with sea surface temperatures (not shown) are everywhere weak and do not pass the pattern-significance test.

The northward excursions of precipitation measured by c (Fig. 6a) are correlated with SLP on the interannual time scale in a pattern (Fig. 6b) that is almost the mirror image of the domain-average correlations (Fig. 5a) in the NH and, especially, over western North America, in accordance with modest anticorrelation between interannual $\overline{p}$ and c ($r = -0.29$). Globally, correlations of c with SLPs are dominated by a broad positive Walker cell circulation, as expected from the positive correlation of c to SOI (Table 2), although only weakly so over the eastern tropical Pacific. Correlations of interannual SST variations with both c (Fig. 6c) and PC 1 (not shown) are highly significant according to the pattern-significance test and resemble the global SST patterns associated with ENSO. The modest correlations over the eastern tropical Pacific may be an artifact of the bandpass filtering which blurs the influences of individual El Niño–La Niña events.

Correlations in Fig. 6b are significant at the centers where $|r| > 0.4$. Regionally, positive c anomalies (northward shifts in zonal precipitation) are correlated with a high-pressure region above and off the California coast, reminiscent of the California Pressure Anomaly (CPA) that Cayan and Peterson (1989) (see their Fig. 13) observed to be well correlated with diminished California precipitation. High pressure in this region shelters California and Oregon from winter storms and generally diverts flow to the north (increasing central latitude). The positive and negative correlations over the North Pacific basin [in both the global SLP set, 1951–92, and in NH SLPs, 1899–1994 (not shown)] trace a quadrapole pattern that encompasses 1) the eastern Pacific pressure dipole that Brown (1995) found to be associated with precipitation anomalies in northwestern and southwestern regions of North America and 2) the western Pacific (WP) (Barnston and Livezey 1987) dipole that reflects the influence of weakening of the western Pacific jet in directing the location of precipitation along the West Coast. Dai and Rasmusson (1996) illustrated a tendency for expansions of the jet to occur along with southward storm track excursions at the West Coast during El Niños. This WP dipole of correlations also is reflected in the correlations of interannual PC 1 (north–south seesaw) and SLP (not shown), which reaffirms

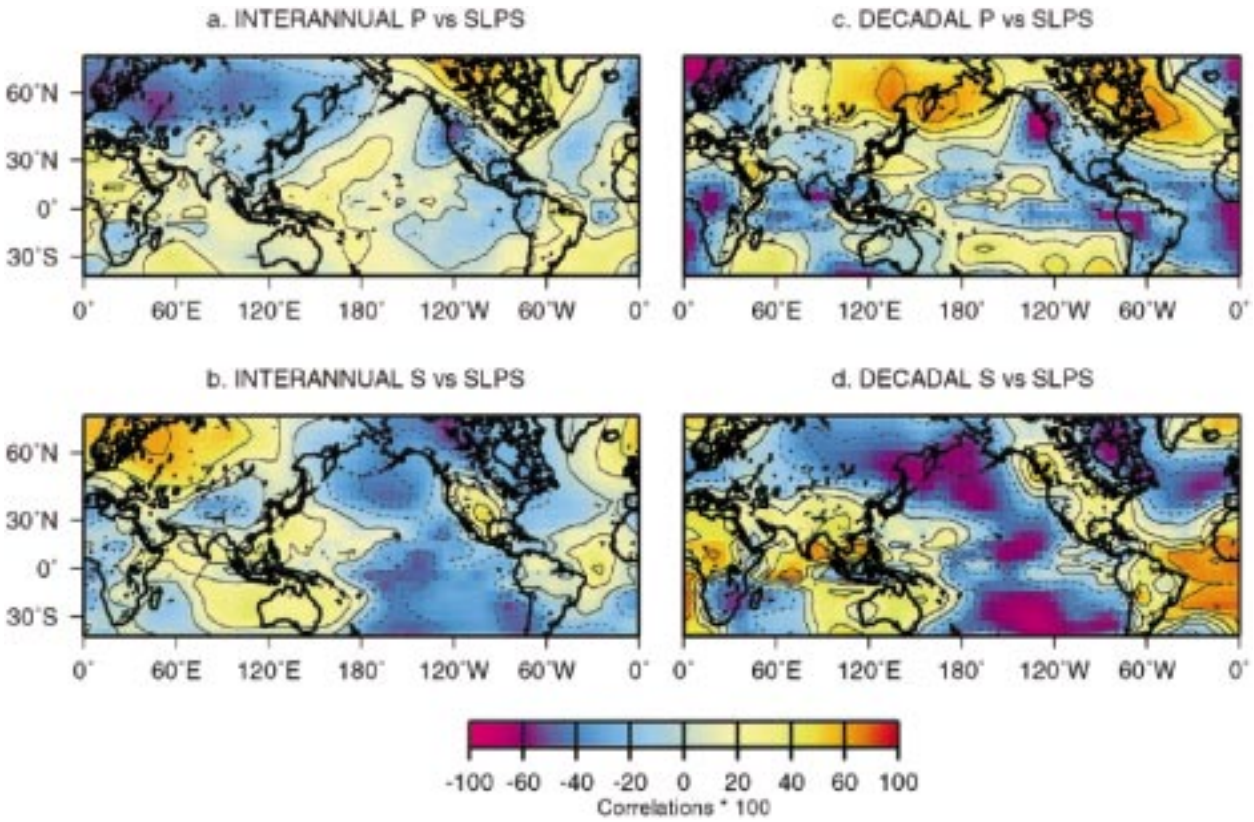

FIG. 5. Correlations (×100) between interannual SLPs and interannual (a) $\overline{p}$ and (b) *s*, and between decadal SLPs and decadal (c) $\overline{p}$ and (d) *s*, 1951–92. Contour interval is 20; dashed where negative.

that this ''distant'' feature plays a relatively consistent role in determining the north–south placement of precipitation along the West Coast on these interannual timescales.

Correlations between interannual latitudinal spread *s* and SLP (Fig. 5b and with respect to longer NH SLP records) form a global Walker cell pattern in keeping with the positive SOI correlations in Table 2 (not quite significant), but are not globally significant by the pattern-significance test. The positive anomaly over Texas in Fig. 5b is not pronounced in correlations with the longer NH SLP record. Correlations with interannual SSTs (not shown) do form a globally significant pattern (at a 98% confidence level) that is a weaker, mirror image of the pattern in Fig. 6c. Thus correlations of interannual *s* and SSTs are dominated by positive correlations of *s* with tropical SSTs, indicating that broader precipitation distributions occur when warm tropical El Niño conditions prevail and narrower distributions occur during La Niñas.

Correlations of decadal SLPs with decadal $\overline{p}$ (Fig. 5c) are not globally significant and are mostly dominated by a CPA-like patch of negative correlations at about 40°N over and offshore from western North America (Cayan and Peterson 1989). This CPA-like patch is similar to the pattern observed in the interannual correlations (Fig. 5a). The control that circulation over this region exerts on $\overline{p}$ is also reflected (weakly) in negative correlations of decadal SSTs in the Gulf of Alaska with $\overline{p}$ (not shown). Together, these correlation patterns suggest that (for negative decadal excursions of $\overline{p}$) the most reliable control on precipitation delivery to the West Coast has been the decadal equivalent of a blocking circulation over the easternmost North Pacific, with long periods in which jets and storms have been displaced northward. In the midst of much short-term variability, from daily to interannual, subtle decadal tendencies to favor circulations that approximate this blocked pattern have modified long-term precipitation totals. Farther from western North America, interannual and decadal correlations are quite dissimilar, and the overall decadal correlation pattern is not statistically significant. As expected from the association of decadal EOF 2 with overall precipitation, the correlations linking $\overline{p}$ with decadal SLP and SST fields are essentially the inverse of those for SLP and decadal PC 2 (not shown).

Correlations between decadal SLPs and *c* (Fig. 6e) are dominated by positive correlations over the entire eastern Pacific, at levels that readily pass pattern-significance tests. Presumably the positive phase of this pattern describes a decadal-average circulation pattern over the North Pacific that favors poleward displace-

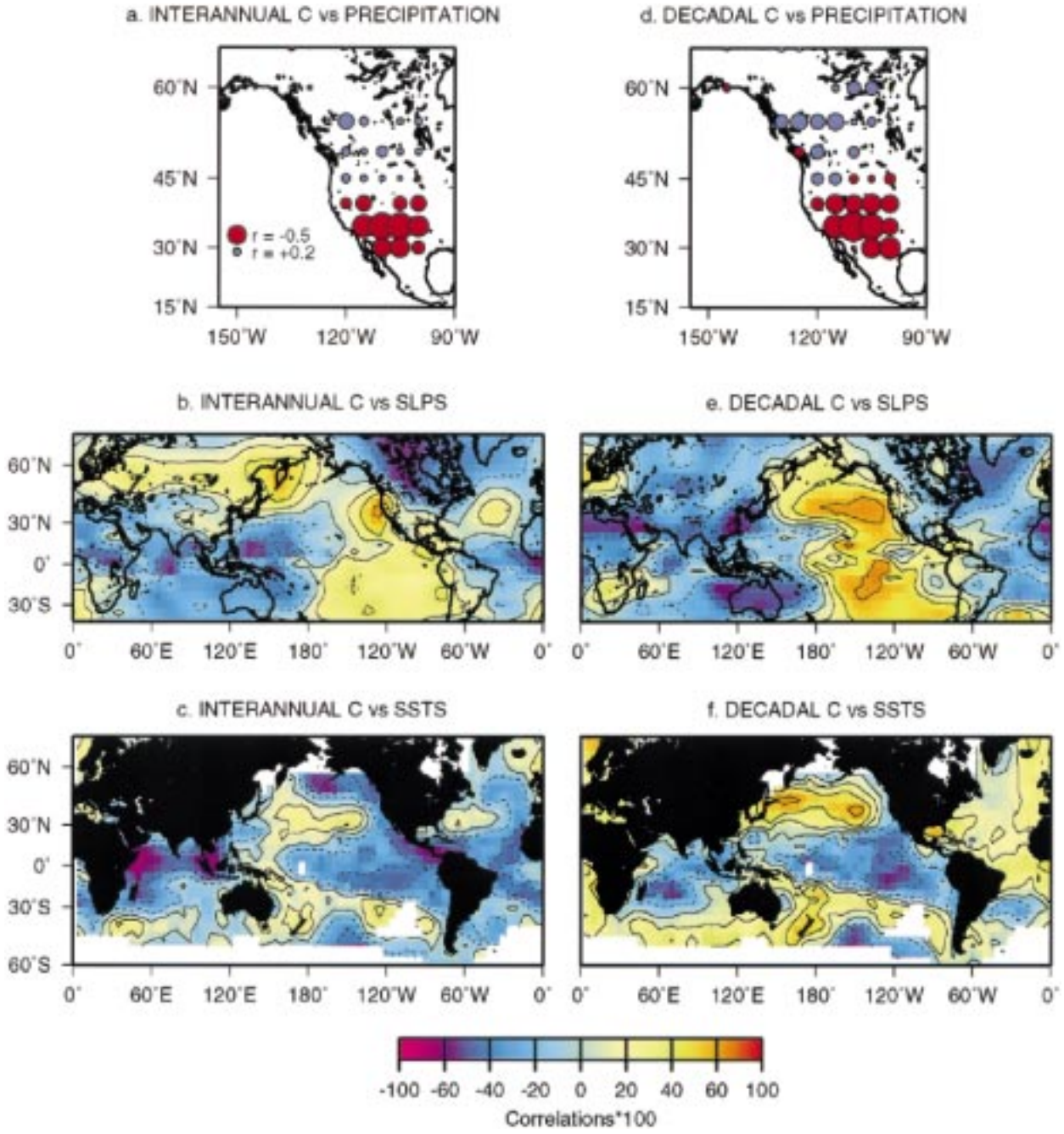

FIG. 6. (a)–(c) Correlations between interannual *c* and (a) interannual, gridded precipitation anomalies, 1901–91 (Eischeid et al. 1991; Eischeid et al. 1995), (b) interannual SLPs, 1951–92, and (c) interannual SSTs, 1901–91. (d)–(f) Same as (a)–(c), except analyzing decadal variations. Contour interval is 20; dashed where negative.

ments of the storms and jets that would produce a northward shift in the precipitation center of mass (Fig. 6d). More broadly, the SLP-correlation pattern is the decadal analog of a strong global La Niña condition wherein pressure over much of the eastern Pacific is higher than normal and pressure over the west is lower. The La Niña analogy is also indicated by correlations with decadal SSTs (Fig. 6f). Conversely, El Niño–like atmospheric circulations (Zhang et al. 1997) are associated with a wet southwestern North America and dry winters farther north. A weak WP dipole appears at the western Pacific edge of this pattern (as in correlations with decadal PC 1), indicating the decadal-average strengthening and weakening of the subtropical jet in the western Pacific influences the north–south placement of precipitation on decadal timescales. Importantly, the decadal patterns

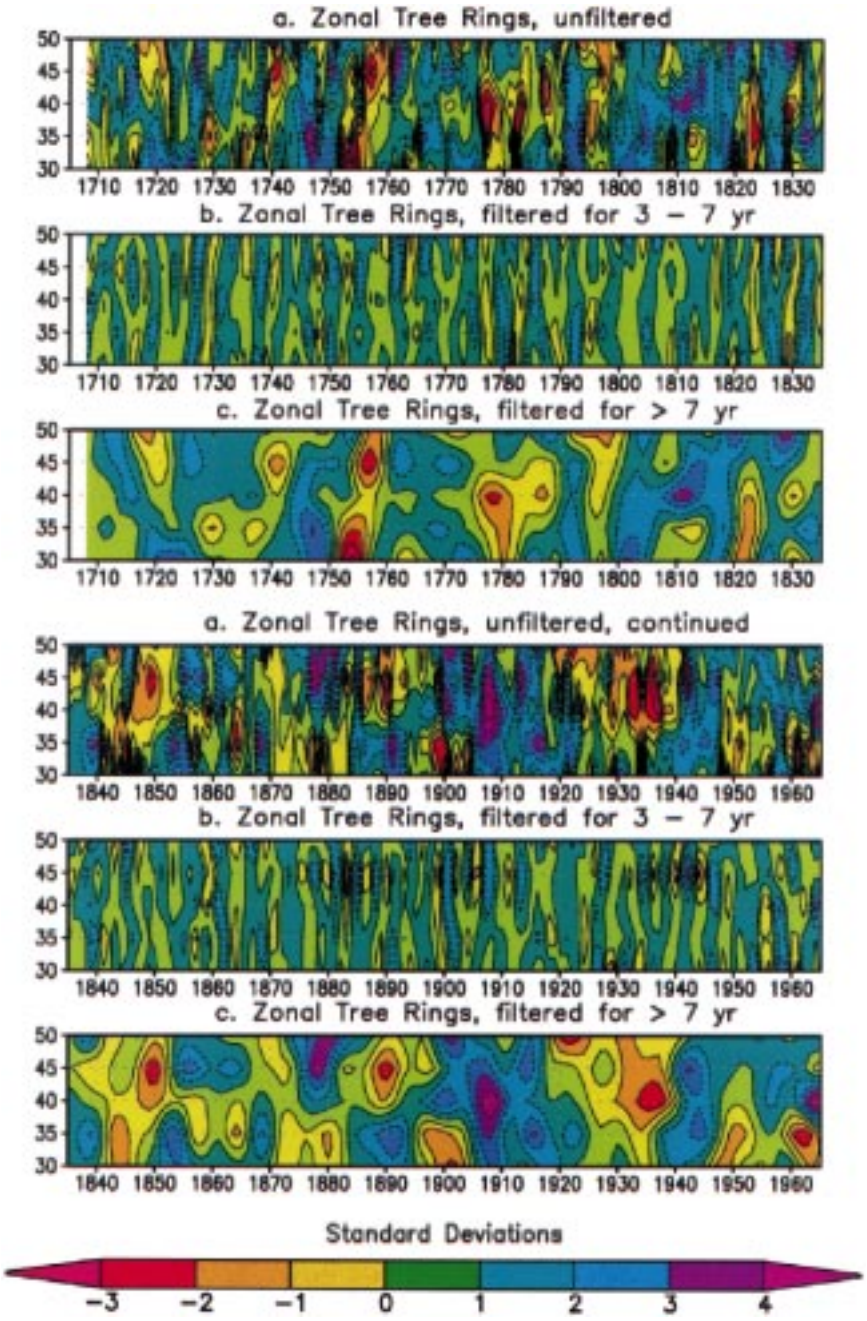

FIG. 7. Time–latitude diagram of zonal tree-ring averages, 1708–1965, for (a) raw, (b) interannual, and (c) decadal tree-ring chronologies.

quite closely resemble the interannual patterns. The global SLP-correlation pattern in Fig. 6e also is essentially the same pattern that has been associated with a decadal global precipitation mode characterized by anomalies over both the Sahel and American southwest (Cayan et al. 1998).

Locally, the correlations between decadal SLPs and s (Fig. 5d) indicate a relation between high pressure anomalies along the northernmost West Coast and latitudinal spread, with a possible ''window'' of lower pressures allowing storm passage nearer 35°–40°N (a pattern that persists when the longer NH SLP set is used). Globally the pattern is quite strong (as indicated by the pattern significance tests) with negative correlations appearing over the central North Pacific (and North Atlantic) and a WP dipole farther west. On decadal timescales, the correlation of s and PC 2 is $+0.68$, and the correlation of s and $\overline{p}$ is -0.47, so that (as noted

earlier) the latitudinal spread of precipitation is linked to controls on the same precipitation totals around 40°N that are measured by PC 2 and $\overline{p}$. As with correlations between decadal SSTs and $\overline{p}$, the correlations between SSTs and *s* are not large or significant.

In summary, the spatial distribution and overall amounts of precipitation in western North America on both interannual and decadal timescales are associated with combinations of local offshore circulations (over the eastern North Pacific), with ENSO-like climatic conditions (e.g., Zhang et al. 1997), and with the WP dipole around the western Pacific subtropical jet. The only consistent controls on precipitation-total amounts are local on both timescales, whereas precipitation's central latitude and latitudinal spread exhibit strong Pacific-wide (and larger) ties on both timescales. Despite a tendency for *c* to correlate with somewhat more distant and more extratropical forcings on decadal timescales, the similarities between the precipitation patterns and climatic forcings associated with central latitude on interannual and decadal timescales, shown in Fig. 6, are particularly striking. This suggests that similar large-scale mechanisms operate to redistribute precipitation latitudinally on both timescales. Similar climatic connections can be gleaned from the EOFs of the zonal precipitation.

6. Tree-ring reflections of the north–south precipitation patterns

Several characteristics of the zonal precipitation series discussed above are reflected in tree-ring chronologies, which provides some confidence that observed spatial characteristics of precipitation variability in western North America are representative of a period longer than the approximate 110-yr instrumental record. In this section, some preliminary comparisons are presented. First, a tree-ring analog of the precipitation-latitude diagrams of Fig. 1 is shown in Fig. 7. These plots are based on averages of normalized tree-ring chronologies from 5° latitude zones from 30° to 50°N and mostly near the coast (described in the data section). Multivariate analyses of the tree rings, together with the zonal-precipitation series and a parallel set of zonal air temperatures, indicate that, while the tree-ring variations are sensitive to precipitation, they are better explained by a complex seasonal mix of precipitation *and* temperatures at each latitude. Despite this complex response, variations of tree-ring chronologies as a function of latitude and time reflect many of the same episodes as found in the (instrumental) zonal-precipitation series (Fig. 1), such as an intensification of interannual variations near 40°–45°N in the early 1940s and the northward decadal spread of drought in the early 1950s.

The spatial patterns in the zonally averaged precipitation, as captured earlier by the EOFs and spatial moments, are reflected in tree-ring series from throughout western North America. Temporal correlations of the domain average $\overline{p}$ and central latitude *c* of the instrumental precipitation series with 140 tree-ring series are shown in Fig. 8, with correlations ranging from −0.5 to +0.4. Tree rings are positively correlated with $\overline{p}$ in northern California and Oregon (Fig. 8a), in accordance with the importance of precipitation in that region to overall western North American precipitation totals (Fig. 4a). Much of the correlation there derives from decadal variations shared by $\overline{p}$ and the thickness of tree rings. Tree-ring thicknesses are anticorrelated with *c* throughout much of the southwestern United States (Fig. 8b). This correlation pattern reflects the north–south seesaw of precipitation as filtered by tree-ring chronologies that are more precipitation sensitive in the southwest than in the northwest. Correlations between filtered tree rings and the interannual and decadal PC series indicate similar relations and range between −0.5 and +0.6.

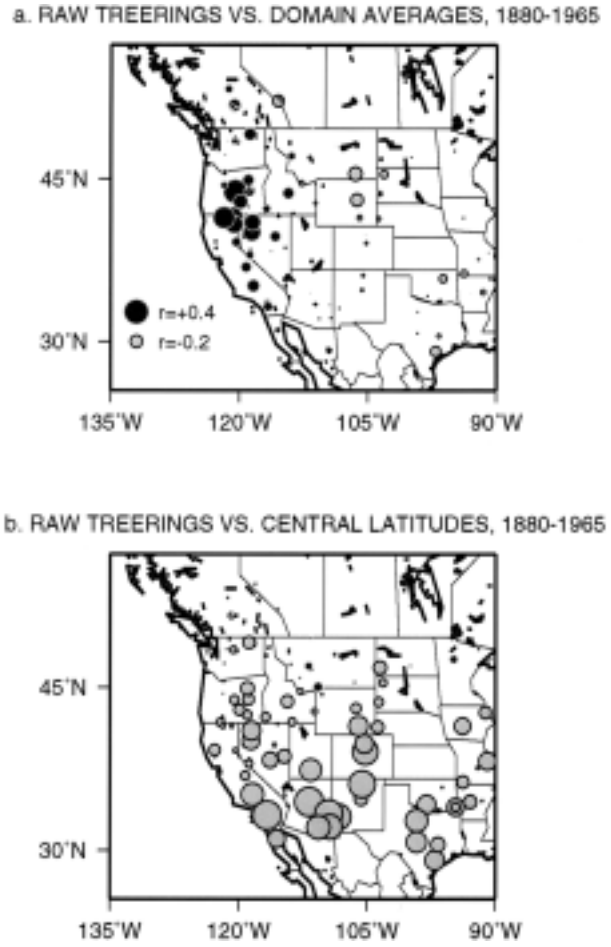

FIG. 8. Correlations between selected interannual tree-ring series and (a) domain average $\overline{p}$, and (b) central latitude *c*, 1880–1965.

Although many of the temporal correlations in Fig. 8 are modest, together the spatial patterns in each of the maps capture significant fractions of long-term variations of the precipitation moments. In particular, if the correlation patterns in Fig. 8 are treated like EOF weights, and year-to-year tree-ring variations are pro-

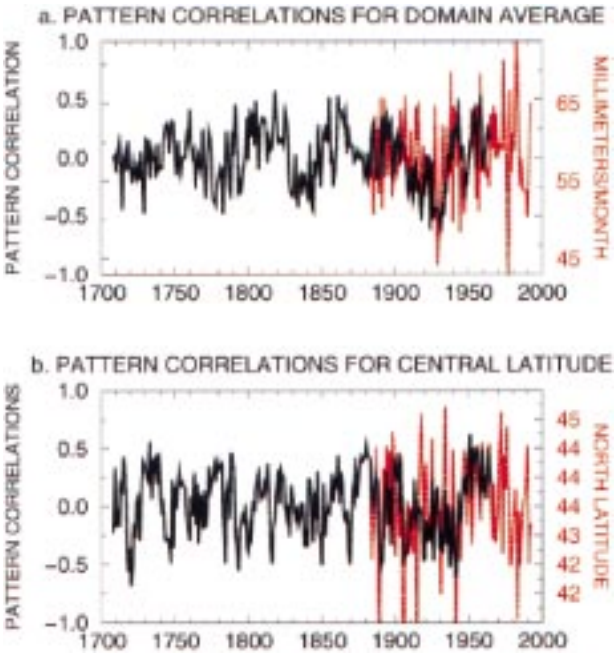

FIG. 9. Pattern correlations of decadal tree-ring series with (a) the temporal correlations in Fig. 8a and (b) the temporal correlations in Fig. 8b for those series west of 100°W longitude. Dotted curve is the associated precipitation moment series; solid curve is the series of pattern correlations.

jected onto them, then the resulting amplitude series (actually, a series of spatial pattern correlations) measures overall similarity of annual tree-ring maps to the patterns in Fig. 8 as a function of time. By this approach, the precipitation moments can be extrapolated back into the past, prior to the instrumental record. Figure 9 shows such pattern-correlation series for domain-average precipitation $\overline{p}$ and central latitude c. During the period when moments and tree rings are available (1880–1965), the pattern-correlation series are well correlated ($r = +0.42$ for $\overline{p}$ and $r = +0.56$ for c, yielding $p < 0.005$ in both cases). When filtered tree rings are projected onto correlation patterns for the decadal moments, the temporal reconstructions of the moments can capture as much as 50% of decadal variance. Prior to the instrumental record, amplitudes and oscillations are present in the pattern correlations that are quite similar to the instrumental records for spatial moments. Similar projections of the zonal PCs onto tree-ring maps also show much similarity between variations of the precipitation patterns before and during the instrumental record. These simple extrapolations suggest that preinstrumental precipitation patterns may have displayed much the same character as those documented by the instrumental record.

One exception to this similarity before and after the beginning of the instrumental record is the apparent increase in very low frequency (VLF) variations with periods greater than about 30 years, for tree-ring reconstructions of both moments, during the last 100 years. This recent increase in VLF variation is present in the individual tree-ring chronologies, as indicated by construction of tree-ring spectral maps (not shown here) and in the precipitation-moment reconstructions; see also Diaz and Pulwarty (1994). All three of these tree-ring measures of precipitation variability show more VLF variation during the interval from about the mid- to late-1800s to 1960 than during the interval from 1700 to 1850. Spectral analyses of a few long tree-ring reconstructions, for example, a millennial series from the Flagstaff area (J. Dean, Tree-Ring Laboratory, The University of Arizona, 1996, personal communication), however, identify periods of VLF variation prior to 1700 that are comparable to the present century. Similar projections of tree-ring correlations with the interannual PCs suggest that tree-ring variations correlated with the higher-frequency precipitation modes continued unabated into the preinstrumental past.

7. Summary and conclusions

An important component of precipitation variability in westernmost North America is characterized by regional north–south contrasts that appear at many timescales. Zonally averaged precipitation variations across this region are studied in terms of how much the regional precipitation amount and distribution vary from year to year and how they relate to large-scale variations as depicted by sea level pressure and sea surface temperature patterns. Two timescales are considered (interannual, 3–7 yr, and decadal, >7 yr). Spatial EOFs of the zonal averages (from 15° to 60°N) and spatial moments (from 25° to 55°N) are analyzed to determine the dominant spatial distributions of precipitation and to identify large-scale climatic settings associated with those precipitation variations. Interannual (3–7 yr) and decadal (>7 yr) timescales are compared.

Zonal patterns (EOFs) of the interannual and decadal filtered versions of the zonal-precipitation series are remarkably similar. At both interannual and decadal timescales, as well as in higher- and lower-frequency bands, the two leading EOFs of zonal precipitation describe 1) a north–south seesaw of precipitation pivoting near 40°N and 2) variations in precipitation near that pivot point, respectively. Analyses of the spatial moments (domain average, central latitude, and latitudinal spread) of zonal precipitation show that domain average is governed mostly by the precipitation mode centered near 40°N. Central latitude is influenced mostly by precipitation in the southern midlatitudes (near 30°–35°N). Central latitude is correlated positively with SOI so that warm periods in the tropical Pacific are associated with southern displacements of the precipitation distribution on both interannual and decadal timescales. Overall precipitation amount (indicated by the domain averages) varies from winter to winter by about 10% of the long-term mean, and no long-term trend or consistent cor-

relations to global-scale climatic forcings were found. Instead, overall amount is only consistently related to circulation conditions immediately offshore from northern California and Oregon. In the interannual band, the central latitude of precipitation anomalies is related to distant tropical and subtropical conditions and pressure anomalies immediately off the West Coast that steer storms north or south of the pivot point at 40°N. On decadal timescales, the central latitude of precipitation is related to very large scale ENSO-like conditions. The latitudinal spread of precipitation along the West Coast increases when the southern zones are anomalously wet (and vice versa) and thus is negatively related to central latitude and its climatic driving forces.

Some temporal features of these precipitation patterns are replicated by using tree-ring series that span some 260 years of precipitation variability within the study region. Comparisons of the long- and short-term variations of zonal averages of the tree-ring series with precipitation patterns during the same periods indicate much shared information. The temporal correlations of tree rings to the precipitation PCs and spatial moments yielded moderate correlations, which can be used with year-to-year tree-ring variations to capture about 25% of the overall variance of the precipitation moments (but as much as 50% in the decadal band). The relatively close correspondence between tree-ring variation patterns and large-scale precipitation patterns suggests avenues for further extending the history of precipitation patterns (and perhaps their climatic forcings) into the preinstrumental past. Meanwhile, the present results suggest that temporal and spatial structure of western North American winter precipitation has been relatively stable for several hundred years.

Do the north–south precipitation patterns reflect changes or redistributions of the overall amount of precipitation delivered to the cordillera of western North America? In general, total winter precipitation varies only by about ±10% from year to year. Within these small variations, on interannual timescales, the north–south dipole of anomalous precipitation and overall amount are anticorrelated, whereas, on decadal timescales, the two are not significantly correlated. Given the strong climatological contrasts in precipitation from the wet northern areas to the dry southern areas, even the overall distribution of precipitation from north to south—as measured by central latitude and latitudinal spread—has varied relatively little. Thus, overall, we find that precipitation delivered to the region has been remarkably stationary during the last 115 yr (and, based on tree-ring pattern correlations, perhaps much longer). For example, sustained intervals (longer than 1 yr in a row) with domain-average precipitation totals greater than 110% of normal or less than 90% of normal occurred only twice during the historical record, in 1929–31 (dry) and 1982–83 (wet). In certain individual years, however, such as 1977 (37% drier than normal) and 1983 (29% wetter than normal), much larger excursions in amount and distribution of precipitation have occurred. Thus, historical precipitation variations only rarely provide us with analogs for regionwide droughts or wet periods of severity comparable to those inferred from paleoclimatic records (e.g., Stine 1994) and certain greenhouse-warming scenarios (e.g., Giorgi et al. 1994).

Do the different precipitation timescales reflect different processes and teleconnections? EOF analyses showed that the dominant spatial patterns of precipitation in western North America are similar almost regardless of the timescale considered, from 2–20 yr. The interannual precipitation patterns are somewhat more consistently associated with local circulation conditions, whereas decadal patterns may tend to reflect conditions from farther afield. However, aspects of the latitudinal distribution of precipitation have associated climatic conditions (SLPs and SSTs) that show many similarities from interannual to decadal timescales (see, especially, Fig. 6, as well as Cayan et al. 1998), Thus, similar large-scale patterns of tropical–extratropical climate are associated with the interannual and decadal precipitation patterns, but with subtle differences, from one timescale to the next, in the spatial scales and locations of the strongest climatic correlations.

Acknowledgments. Comments by David Peterson and Lauren Hay, USGS; Dan Moore of Simon Fraser University; Martin Hoerling, NOAA/Climate Diagnostics Center; and three anonymous reviewers improved this paper. Emelia Bainto, Scripps Institution of Oceanography, provided preliminary versions of the figures, many of which were made with the GMT system (Wessel and Smith 1991). Jon Eischeid, NOAA CDC, provided historical records of precipitation and graphical assistance, and Jefferey Dean, The University of Arizona, provided millenial tree-ring series from the Flagstaff area. The 1995 PACLIM Workshop provided a forum for the initial presentation of some of this material. This study was supported by a grant from the NOAA Paleoclimatology Program Grant NA56GPO404 and the USGS Global Change Hydrology Program. Drought aspects were motivated by issues being addressed in the USGS San Francisco Bay Ecosystems Initiative and NOAA's interest in water resources issues related to climatic variability.

REFERENCES

Barnett, T. P., K. Brennecke, J. Limm, and A. M. Tubbs, 1984: Construction of a near-global sea-level pressure field. Scripps Inst. Oceanogr. Reference Series 84-7, 35 pp. [Available from Scripps Institution of Oceanography, La Jolla, CA 92093.]

Barnston, A. P., and R. E. Livezey, 1987: Classification, seasonality and persistence of low-frequency atmospheric circulation patterns. *Mon. Wea. Rev.*, **115,** 1083–1126.

Brown, T. J., 1995: Long-wave circulation patterns associated with winter-time precipitation departures over western North America. Ph.D. thesis, University of Colorado, 197 pp.

California Department of Water Resources, 1978: *The 1976–1977 California Drought—A review*. California Resources Agency,

Department of Water Resources, 228 pp. [Available from California Dept. of Water Resources, 3310 El Camino, Sacramento, CA 95821.]

Cayan, D. R., and D. H. Peterson, 1989: The influence of North Pacific atmospheric circulation on streamflow in the West. *Aspects of Climate Variability in the Pacific and Western Americas, Geophys. Monogr.,* No. 55, Amer. Geophys. Union, 375–396.

——, and R. H. Webb, 1992: El Niño/Southern Oscillation and streamflow in the western United States. *El Niño—Historical and Paleoclimatic Aspects of the Southern Oscillation,* H. F. Diaz and V. Markgraf, Eds., Cambridge University Press, 29–68.

——, M. D. Dettinger, H. F. Diaz, and N. Graham, 1998: Decadal variability of precipitation over western North America. *J. Climate,* **11,** 3148–3166.

Dai, Z., and E. M. Rasmusson, 1996: ENSO cycle modulation of transient behavior over the North Pacific-North American sector. Preprints, *Eighth Conf. on Air–Sea Interaction and Symp. on the Global Ocean-Atmosphere-Land System (GOALS),* Phoenix, AZ, Amer. Meteor. Soc., 356–369.

Dettinger, M. D., M. Ghil, and C. L. Keppenne, 1995a: Interannual and interdecadal variability of United States surface-air temperatures, 1910–1987. *Climate Change,* **31,** 35–66.

——, ——, C. M. Strong, W. Weibel, and P. Yiou, 1995b: Software expedites singular-spectrum analysis of noisy time series. *Eos, Trans. Amer. Geophys. Union,* **76,** 12, 14, 21.

Diaz, H. F., and V. Markgraf, 1992: *El Niño—Historical and Paleoclimatic Aspects of the Southern Oscillation.* Cambridge University Press, 476 pp.

——, and R. S. Pulwarty, 1994: An analysis of the time scales of variability in centuries-long ENSO-sensitive records. *Climate Change,* **26,** 317–342.

Eischeid, J. K., H. F. Diaz, R. S. Bradley, and P. D. Jones, 1991: A comprehensive precipitation data set for global land areas. DOE/ER-69017T-H1, TR051, 81 pp. [Available from NTIS, U.S. Dept. of Commerce, Springfield, VA 22161.]

——, C. B. Baker, T. R. Karl, and H. F. Diaz, 1995: The quality control of long-term climatological data using objective data analysis. *J. Appl. Meteor.,* **34,** 2787–2795.

Giorgi, F., C. Shields Brodeur, and G. T. Bates, 1994: Regional climate change scenarios over the United States produced with a nested regional climate model: Spatial and seasonal characteristics. *J. Climate,* **7,** 375–399.

Gleick, P. H., and L. Nash, 1991: The societal and environmental costs of the continuing California drought. Pacific Institute for Studies in Development, Environment, and Security Research Rep., 66 pp. [Available from Pacific Institute, 654 13th St., Oakland, CA 94612.]

Hurrell, J. W., 1995: Decadal trends in the North Atlantic oscillation: Regional temperatures and precipitation. *Science,* **269,** 676–679.

Jiang, N., D. Neelin, and M. Ghil, 1995: Quasi-quadrennial and quasi-biennial variability in the equatorial Pacific. *Climate Dyn.,* **12,** 101–112.

Kaylor, R. E., 1997: Filtering and decimation of digital time series. Inst. Phys Sci and Tech. Tech. Rep. BN850, 14 pp. [Available from Engineering and Physical Science Laboratory, University of Maryland at College Park, College Park, MD 20740.]

Kiladis, G. N., and H. F. Diaz, 1989: Global climatic anomalies associated with extremes of the Southern Oscillation. *J. Climate,* **2,** 1069–1090.

Latif, M., and T. P. Barnett, 1996: Decadal climate variability over the North Pacific and North America: Dynamics and predictability. *J. Climate,* **9,** 2407–2423.

Lees, J., and J. Park, 1995: Multiple-taper spectral analysis: A standalone C subroutine. *Comput. Geosci.,* **21,** 199–236.

Lott, N., D. Ross, and M. Sittel, 1997: The winter of '96–'97 West Coast flooding. Research Customer Service Group Tech. Rep. 97-01, National Climate Data Center, 23 pp. [Available online from orders@ncdc.noaa.gov.]

Meko, D. M., E. R. Cook, D. W. Stahle, C. W. Stockton, and M. K. Hughes, 1993: Spatial patterns of tree-growth anomalies in the United States and southeastern Canada. *J. Climate,* **6,** 1773–1786.

Mitchell, T. P., and W. Blier, 1997: The variability of wintertime precipitation in the region of California. *J. Climate,* **10,** 2261–2276.

Nichols, F. H., J. K. Thompson, and L. E. Schemel, 1990: The remarkable invasion of San Francisco Bay (California, USA) by the Asian clam *Potamocorbula amurensis,* II. Displacement of a former community. *Mar. Ecolog. Prog. Ser.,* **66,** 95–101.

Parker, D. E., C. K. Folland, A. Bevan, M. N. Ward, M. Jackson, and K. Maskell, 1995: Marine surface data for analysis of climatic fluctuations on interannual to century timescales. *Natural Climate Variability on Decade-to-Century Time Scales,* D. G. Martinson et al., Eds, Climate Research Committee, National Research Council, National Academy Press, 241–250.

Percival, D. B., and A. T. Walden, 1993: *Spectral Analysis for Physical Applications—Multitaper and Conventional Univariate Techniques.* Cambridge University Press, 580 pp.

Philander, S. G., 1990: *El Niño, La Niña, and the Southern Oscillation.* Academic Press, 289 pp.

Riehl, H., 1981: The limits of the subtropical jet stream. *Contrib. Atmos. Phys.,* **54,** 335–351.

Stine, S., 1994: Extreme and persistent drought in California and Patagonia during medieval time. *Nature,* **369,** 546–549.

Ting, M., M. P. Hoerling, T. Xu, and A. Kumar, 1996: Northern Hemisphere teleconnection patterns during extreme phases of the zonal-mean circulation. *J. Climate,* **9,** 2614–2633.

Trenberth, K. E., and D. A. Paolino, 1980: The Northern Hemisphere sea-level pressure data set trends, errors, and discontinuities. *Mon. Wea. Rev.,* **108,** 855–872.

——, and J. W. Hurrell, 1994: Decadal atmospheric–ocean variations in the Pacific. *Climate Dyn.,* **9,** 303–319.

Wessel, P., and W. H. F. Smith, 1991: Free software helps map and display data. *Eos, Trans. Amer. Geophys. Union,* **72,** 441, 445–446.

White, W. B., and Y. M. Tourre, 1995: ENSO signals in global upper ocean temperature. *J. Phys. Oceanogr.,* **25,** 1317–1332.

Zhang, Y., J. M. Wallace, and D. S. Battisti, 1997: ENSO-like interdecadal variability: 1900–93. *J. Climate,* **10,** 1004–1020.

Zorita, E., V. Kharin, and H. von Storch, 1992: The atmospheric circulation and sea surface temperature in the North Atlantic area in winter: Their interaction and relevance for Iberian precipitation. *J. Climate,* **5,** 1097–1108.